IEEE Access
Multidisciplinary | Rapid Review | Open Access Journal

Received 4 March 2024, accepted 29 April 2024, date of publication 8 May 2024, date of current version 24 May 2024.

Digital Object Identifier 10.1109/ACCESS.2024.3397923

RESEARCH ARTICLE

Design and Analysis of a New Excitation Structure for Magnetron Sputtering

ZE-DA SU[1], YUE-JUN AN[1], HUI AN[1], YAN-JUN LU[2], WEN-YU DENG[3], LI-JUN QI[3], AND MING LI[1,4]

[1]School of Electrical Engineering, Shenyang University of Technology, Shenyang 110870, China
[2]Shenyang KINGSEMI Company Ltd., Shenyang 110168, China
[3]Shenyang China North Vacuum Equipment Company Ltd., Shenyang 110159, China
[4]College of Control Science and Engineering, Bohai University, Jinzhou 121013, China

Corresponding author: Ze-Da Su (2639324505@qq.com)

This work was supported by Liaoning Provincial Science and Technology Program Project under Grant 2023JH1/11100010.

ABSTRACT Magnetron sputtering systems are widely used for depositing industrially important coatings. Research has been conducted to optimize and improve these structures to increase coating effectiveness and target utilization. The paper investigates the engineering problem of uneven target etching caused by an uneven magnetic field in magnetron sputtering equipment. The characteristics of the desired magnetic field distribution required by magnetron sputtering equipment are analyzed, and a corresponding excitation structure and analytical model for cylindrical magnetron sputtering equipment are proposed and calculated. The uniform magnetic field design is realized by analytical modeling of the excitation structure. The axial magnetic field distributions produced by an axisymmetric solenoid system and several similar excitation structures are analyzed and compared. The analytical results were verified through finite element simulations and experiments, demonstrating the accuracy and effectiveness of the method. The excitation structure, which is designed with a uniform magnetic field, can produce an axial component of magnetic flux density with a uniformity deviation of less than 4.3% across 73% of the target surface. The analytical model describes the distribution of the axial component of the magnetic flux density and optimizes the magnetic field. The model enables the simulation of plasma distribution and film growth, aiming to enhance the target utilization rate and substrate deposition rate. The conclusions serve as a reference for designing high-performance magnetron sputtering equipment.

INDEX TERMS Axisymmetric solenoidal excitation structure, cylindrical magnetron sputtering, high uniformity magnetic field distribution, uniform magnetic field design.

I. INTRODUCTION

To enhance the sputtering rate of diode sputtering and decrease the glow discharge conditions and high temperature of the substrate, magnetron sputtering equipment was developed by introducing a magnetic field to the diode sputtering process [1], [2], [3], [4], [5]. This technology offers the benefits of high deposition rate and low temperature sputtering, and is now widely utilized in various coating industries.

Magnetron sputtering equipment has a high deposition rate because the target surface-parallel magnetic field effectively traps secondary electrons, enhancing the plasma density and the flux of incident ions responsible for sputtering. The introduced magnetic field directly affects the plasma distribution, energy transfer process, target etching morphology, and target utilization [6]. These characteristics are considered to be critical factors in magnetron sputtering equipment, so it is particularly important to analyze and study the characteristics of the desired magnetic field distribution in magnetron sputtering equipment.

Several studies have been conducted on planar and cylindrical magnetron sputtering equipment with various excitation structures. In their work, C.T. Liu et al. proposed a method to enhance the magnetic field distribution and electron trajectories inside magnetron sputtering. This

The associate editor coordinating the review of this manuscript and approving it for publication was Claudio Zunino.

method resulted in improved target utilization, sputtering efficiency, and substrate deposition rate [7], [8]. In a separate study [9], Liu et al. analyzed the impact of magnetic and electric fields on the uniform deposition of target atoms. They also simulated the collision process that occurs in the vacuum cavity. In their work [10], [11], C. T. Liu et al. improved the magnetic field distribution in a DC magnetron sputtering equipment by using passive magnetic shims and an active compensating excitation source. This resulted in increased sputtering of target atoms and a smoother coating. The researchers used two adjustable coils with casters to excite and generate a uniform axial magnetic field in a cylindrical magnetron sputtering apparatus. In their study [12], Kawasaki et al. prepared aluminum alloy A6061 on a cylindrical tube made of carbide steel using magnetron sputtering equipment. They achieved a smooth surface topography and improved film uniformity by generating a modulated magnetic field with a low-frequency alternating coil current. In [13], Wang et al. proposed three ring-shaped permanent magnets excitation structure for a large-diameter tubular workpiece and verified it through finite element simulations. This structure can generate a uniform axial magnetic field in approximately 40% of the area. In [14] and [15], a Helmholtz coil was used to excite a cylindrical magnetron sputtering device, and the resulting plasma distribution and coating effects were investigated. In [16] a three-ring permanent magnet excitation structure was used to excite a cylindrical magnetron sputtering device and the magnetic field related properties were simulated, calculated and analyzed. The excitation structure for magnetron sputtering tends to utilize toroidal permanent magnets [17], long straight solenoids [18], and two coils in an axisymmetric structure, i.e., the Helmholtz coil structure. However, Toroidal permanent magnets can produce a relatively uniform magnetic field distribution in the far axis region, but the uniform magnetic field effect is not ideal and it is difficult to adjust the magnetic field distribution more precisely. The uniformity of the magnetic field produced by a long straight solenoid is also unsatisfactory. Helmholtz coils can only produce a uniform magnetic field in the region close to the axis, not in the region away from the central axis. In addition, several studies have been carried out to optimise and analyse the performance of magnetron sputtering systems using magnetic excitation [19], [20], [21].

This unique electron trapping feature in magnetron sputtering often leads to undesirable target etching, resulting in target waste. In the above study, it was analyzed that the desired magnetic field of magnetron sputtering equipment tends to have the following characteristics:

1. To achieve the desired effect of restraining electrons and increasing plasma concentration, the magnetic field must form a closed tunnel-like distribution above the target surface.

2. The sputtering process occurs more uniformly when the parallel magnetic field components above the target surface are more uniform.

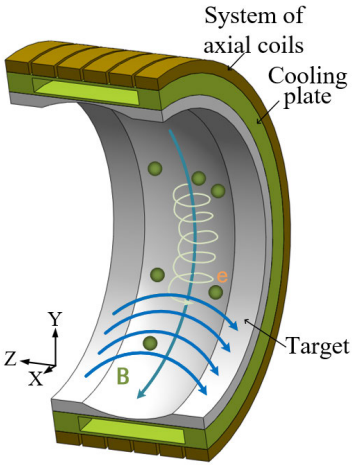

FIGURE 1. Structure of cylindrical magnetron sputtering equipment.

3. The target surface should be covered by the uniform magnetic field as extensively as possible.

The research and development of structures for the uniform excitation of magnetic fields has been going on for many years. Among these, Helmholtz coils and axisymmetric solenoid excitation structures for the generation of uniform magnetic fields are widely used in medicine [22], [23], magnetic resonance imaging [24], [25] and industry [26], [27]. However, such excitation structures for magnetron sputtering equipment have been little studied. In addition, due to different application scenarios, there is an obvious difference in the focus of the region and the shape of the uniform magnetic field generated. Existing research into the use of axisymmetric solenoid excitation structures for uniform magnetic fields focuses on the uniform magnetic field in the spherical region, the uniform magnetic field on the central axis and the uniform magnetic field in the near-axis region. And for cylindrical magnetron sputtering systems, it's necessary to design a uniform magnetic field in the far-axis region. Few studies have been done on this part at present.

For the problem of uniform magnetic field in the far-axis region of cylindrical magnetron sputtering systems. In this paper, based on the distribution characteristics of the desired magnetic field required by the analysed magnetron sputtering equipment, an axisymmetric solenoid system with uniform magnetic field excitation structure applied to cylindrical magnetron sputtering equipment is proposed in Section II. Section III presents definitions and meanings of the parameters of the structure, as well as a thorough analysis of the effects of variations in each parameter. An analytical model of the excitation structure of this axisymmetric solenoid system is also developed and described in detail. In section IV, we design an excitation structure for a magnetron sputtering device that achieves a highly uniform magnetic field. Its validity has been confirmed by finite element calculations and experiments in section V. Section VI compares and analyses several similar excitation structures with the

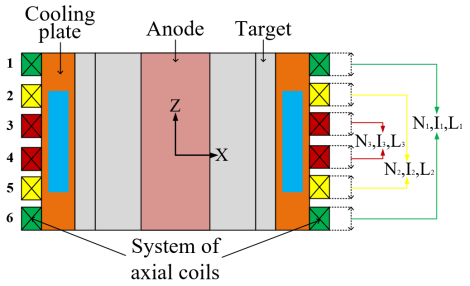

FIGURE 2. Schematic structure of axisymmetric solenoid system.

axisymmetric solenoid system. Finally, section VII presents the conclusions.

II. EXCITATION STRUCTURE OF AXISYMMETRIC SOLENOIDAL SYSTEMS

A. TOPOLOGY OF AXISYMMETRIC SOLENOIDAL SYSTEMS

In current coating technology for tubular workpieces, magnetic field excitation is typically achieved using permanent magnets or solenoids. However, the resulting magnetic field from fixed magnets or solenoids and fixed target structures is often non-uniform. To achieve a greater degree of uniformity in the magnetic field, yokes or permeable shims must be designed. The rotating target structure employs a similar excitation method to the planar target excitation method. However, it requires an additional drive device, such as a motor, to achieve the rotation of the target material, the conductive line, and the cooling water channel. This necessitates the use of slip rings and other devices, which increases the complexity and cost of the equipment. In contrast, solenoids are easier to produce, install, and shape the magnetic field better. If a uniform magnetic field is achieved, it can result in high levels of uniformity in both the magnetic field and target coverage without the need for rotating structures. While the use of solenoid excitation may increase economic costs, the benefits of achieving a uniform magnetic field are significant.

This paper presents an excitation structure for an axisymmetric solenoid system consisting of six sets of solenoids with planar symmetry. Fig.1 illustrates the structure of a magnetron sputtering device with this excitation structure and describes the mechanism of operation of the axisymmetric solenoid system.

The magnetic field distribution that forms a magnetic tunnel enclosing the head and tail within the inner cavity of the cylindrical target is produced by the excitation structure. A significant number of electrons in the vicinity of the target are confined within the magnetic tunnel and continuously collide with gas atoms. The electrons in the tunnel are not easily released, resulting in a high concentration of plasma and a high sputtering rate in magnetron sputtering. The target material is entirely located within the magnetic tunnel coverage. The proposed excitation structure in this paper can significantly enhance the uniformity of the parallel magnetic field component on the target surface by means of uniform magnetic field design. This achieves the goal of improving target utilization and reducing production costs.

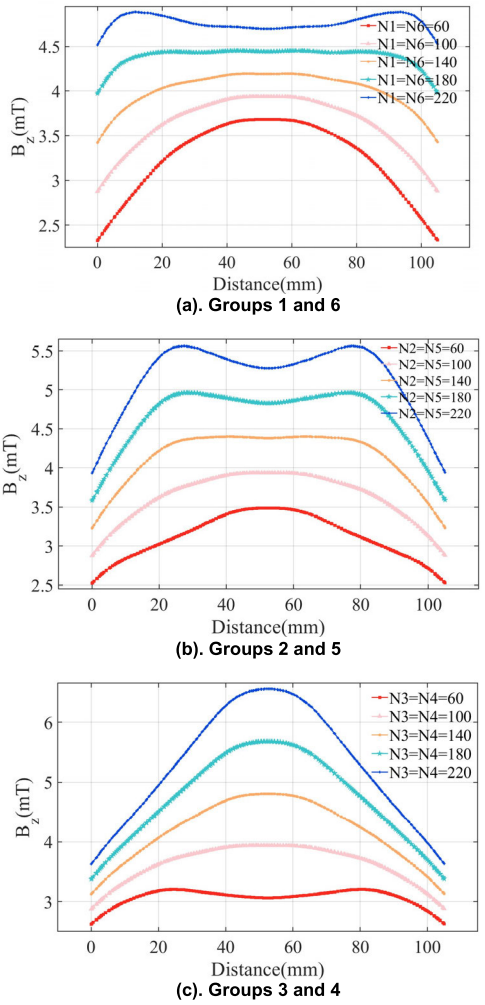

FIGURE 3. Magnetic field distribution curves are affected by changes in the number of turns.

B. DEFINITION OF PARAMETERS

Fig.2 displays six sets of solenoids arranged axially along the structure. All six sets have the z-axis as their axis of symmetry and the geometric center of the structure as their origin. The upper three solenoids and the lower three solenoids are symmetric about the xoy plane and have plane symmetry.

Fig.2 displays the solenoids labeled as group 1 and 6 in green, group 2 and 5 in yellow, and group 3 and 4 in red. The number of turns, current value, and axial length of group 1 and 6 are represented by N_1, I_1, and L_1, respectively. Similarly, N_2, I_2, and L_2 represent the number of turns, current value, and axial length of group 2 and 5, respectively, while N_3, I_3, and L_3 represent the number of turns, current value, and axial length of group 3 and 4, respectively. It is noteworthy that all six groups of solenoids have equal radii and the same current direction.

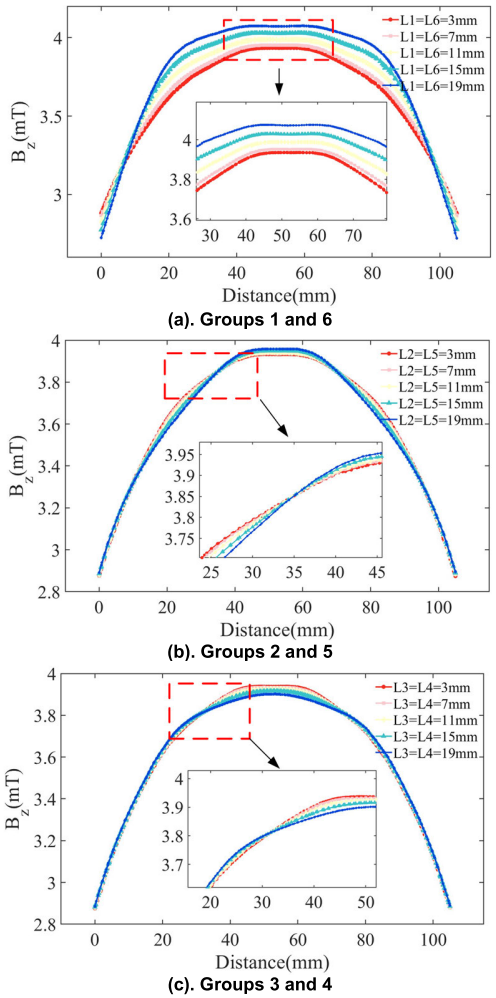

FIGURE 4. Magnetic field distribution curve for axial length variation.

The system comprises of six sets of axisymmetric solenoids that are powered by three DC sources. The magnetic field generated in the axial direction can be regulated by adjusting the three sets of currents, the number of turns, the length of the solenoids. To provide a more comprehensive explanation of the impact of each parameter on the axial magnetic field, we use an axisymmetric solenoid system as an example. The system has a diameter of 100mm, a total axial length of 100mm, and $N_1 = N_2 = N_3 = N_4 = N_5 = N_6 = 100$, $L_1 = L_2 = L_3 = L_4 = L_5 = L_6 = 5$mm, and $I_1 = I_2 = I_3 = I_4 = I_5 = I_6 = 1$A. Because this paper studies the magnetic field in the far-axis region of the cylindrical magnetron sputtering device, the magnetic field distribution curve of the cross-section at 80 mm from the central axis is analyzed here, and Fig.3 shows the magnetic field distribution curve when the number of turns of the six sets of solenoids is changed.

Fig.3(a) shows that increasing the number of turns in groups 1 and group 6, located at the two ends of the device, significantly elevates the magnetic field at the edges of both sides. This can improve the uniformity of the magnetic field.

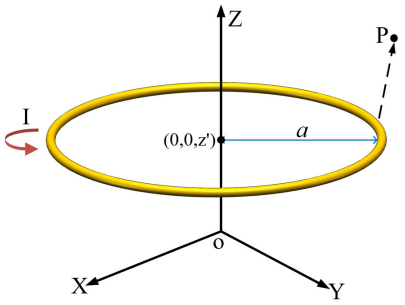

FIGURE 5. Schematic diagram of a circular coil.

However, a non-uniform distribution can also be observed in the middle of the magnetic field curve when N_1 and N_6 are both equal to 180, despite the overall homogeneity. Fig.3(b) demonstrates that increasing the number of turns in groups 2 and group 5 results in a more uniform and stronger magnetic field on both sides. However, the interval of magnetic field improvement is shifted towards the center. When the number of turns of groups 3 and group 4 located in the middle of the device is increased, the magnetic field distribution in the middle increases significantly, while the magnetic field changes on both sides are smaller. Fig.4 displays the curves of the magnetic field distribution as the axial length of the six sets of solenoids is altered.

Fig.4(a) shows that as the axial length of group 1 and group 6 increases, the magnetic field distribution curves in the range of 10-90 mm become gradually more horizontal, while the magnetic field distribution at both ends becomes steeper. In Fig.4(b), there seems to be a difference in the magnetic field distribution curves at 35 mm when the axial length of group 2 and group 5 is varied. The magnetic field decreases with increasing axial length in the region smaller than 35 mm, and the opposite is true in the middle region. In contrast, when the axial lengths of groups 3 and 4, located in the middle of the device in Fig.4(c), are increased, the magnetic field distribution curves exhibit an opposite trend to that shown in Fig.4(b).

The comparison above shows that changes to the parameters will significantly impact the overall magnetic field distribution. In this case, the number of turns has a greater magnitude of effect on the uniformity of the magnetic field, and the change in axial length has a more detailed effect on the uniformity of the magnetic field. The uniformity of the magnetic field can be roughly adjusted by changing the number of turns. Fine adjustment of the magnetic field uniformity is possible by adjusting the axial length. However, the number of turns can be easily adjusted after production. The axial length is fixed prior to manufacture by the installation of shims or other size-fixing devices, and cannot be easily adjusted after manufacture. This indicates that adjusting the parameter combination can result in a highly uniform magnetic field distribution. However, it is worth noting that achieving a high level of uniformity in the magnetic field distribution through multi-parameter tuning may require additional modelling and

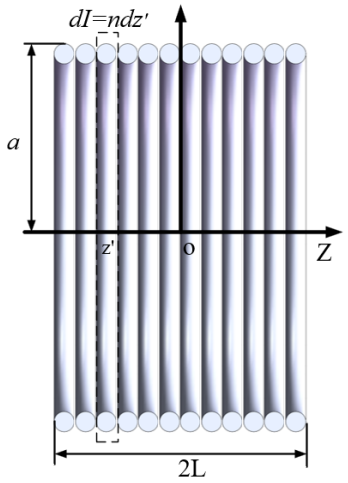

FIGURE 6. Schematic diagram of solenoid.

computational time. Therefore, it is important to perform analytical calculations of the magnetic field generated by this structure. Furthermore, the concentration and spatial distribution of plasma within the magnetron sputtering equipment are dependent on the applied magnetic field [28]. The magnetic field generated by this structure allows for local regulation of the plasma, thereby controlling its distribution in space. Therefore, calculating the magnetic field generated by this structure is significant. The analytical calculation can provide a visual representation of the desired magnetic field distribution and related parameters. This can lead to obtaining a set of appropriate parameter combinations to achieve a uniform plasma density, resulting in a uniform coating.

III. ANALYTICAL MODEL OF THE MAGNETIC FIELD DISTRIBUTION OF AN AXISYMMETRIC SOLENOIDAL EXCITATION STRUCTURE

A. ANALYTICAL OF THE MAGNETIC FIELD DISTRIBUTION OF A TOROIDAL COIL

The magnetic field distribution of any coil with an axisymmetric structure in a constant magnetic field can be calculated using the analytical formula for a single toroidal coil. Therefore, in general, the magnetic field of complex axisymmetric solenoids is often analyzed from the analytical equation of a single toroidal coil.

In general, the centre of the toroidal coil does not coincide with the origin, the radius of the toroidal coil is a and the current is I. The centre of the toroidal coil is located at (0, 0, z'), parallel to the xoy plane, as shown in Fig.5.

Before performing the magnetic field calculations, a theoretical simplification of the model is performed. In the following computational analysis in this paper it is assumed [21], [26] that

1. a single-turn coil with a wire radius much smaller than the coil radius is regarded as an idealized coil with an infinitely small wire radius.

2. each turn of the coil of the solenoid is a coaxial circular loop.

3. the coil is wound uniformly, resulting in a uniform distribution of current density along the cross-section. The direction of the current forms a right-handed helix with the positive direction of the axis of symmetry.

The magnetic vector potential A_1 of the toroidal coil at any point $P(\rho', \varphi', z')$ in space, as well as the axial component B_{1z} of the magnetic flux density, can be expressed in the cylindrical coordinate system.

$$A_1 = A_{1\varphi} = \frac{\mu_0 Ia}{2\pi}\int_0^{\pi}\frac{\cos\phi}{\sqrt{\rho^2+a^2+(z-z')^2-2a\rho\cos\phi}}d\phi \quad (1)$$

$$B_{1z}=\frac{1}{\rho}\frac{\partial(\rho A_1)}{\partial\rho} =\frac{A_1}{\rho}+\frac{\mu_0 Ia}{2\pi}\int_0^{\pi}\frac{(a\cos\phi-\rho)\cos\phi}{\left(\rho^2+a^2+(z-z')^2-2a\rho\cos\phi\right)^{3/2}}d\phi \quad (2)$$

where $A_{1\varphi}$ is the circumferential component of the magnetic vector potential and μ_0 is the air permeability. In this case, the magnetic vector potential of a toroidal coil has only a circumferential component, and both the axial and radial components are zero. This conclusion not only applies to toroidal coils, but also remains valid for more complex axisymmetric solenoid structures. Because any axisymmetric solenoid can be obtained by integrating with a toroidal coil.

B. ANALYTICAL MODEL OF SOLENOIDAL MAGNETIC FIELD DISTRIBUTION

Because the magnetic field generated by the solenoid has axial symmetry, in the analytical solution, it is only necessary to select an axial plane for the magnetic field analysis and calculation. This allows obtaining the magnetic field distribution at the same radial coordinates across the entire circumference.

Set the number of turns per unit length of the solenoid as $n = N/L$, the axial length is $2L$, the z-axis is its axis of symmetry, the xoy plane is its perpendicular plane, as shown in Fig.6. Take the z-axis from the origin o for z' at the width dz' of the current element d$I = nI$dz', d$I = nI$dz'substitution (1) and the (2) in the I, and z' integral, exchange the order of integration can be obtained

$$A_2 = A_{2\varphi} = \frac{\mu_0 nIa}{2\pi}\int_0^{\pi}\int_{-L}^{L}\frac{\cos\phi dz'}{\sqrt{\rho^2+a^2+(z-z')^2-2a\rho\cos\phi}}d\phi \quad (3)$$

$$B_{2z}=\int_{-L}^{L}\frac{A_2}{\rho}dz' + \frac{\mu_0 nIa}{2\pi}\int_0^{\pi}\int_{-L}^{L}\frac{(a\cos\phi-\rho)\cos\phi dz'}{\left(\rho^2+a^2+(z-z')^2-2a\rho\cos\phi\right)^{3/2}}d\phi \quad (4)$$

TABLE 1. Magnetic field distribution curve for axial length variation.

z	15 Intervals	16 Intervals	50 Intervals
0	3.870946	3.870944	3.870941
0.1	3.832559	3.832557	3.832551
0.2	3.708502	3.708501	3.708500
0.3	3.468482	3.468481	3.468480
0.4	3.058952	3.058951	3.058950
0.5	2.467181	2.467180	2.467178

Integrating z' from (3) and (4) yields

$$A_{2\varphi} = \frac{\mu_0 nI}{2\pi} \cdot \int_0^{\pi} \frac{a^2\rho\sin^2\phi}{R^2}\left[\frac{z+L}{\sqrt{(z+L)^2+R^2}} - \frac{z-L}{\sqrt{(z-L)^2+R^2}}\right]d\phi \tag{5}$$

Substitute (5) for (2).

$$B_{2z} = \frac{\mu_0 nI}{2\pi} \cdot \int_0^{\pi} \frac{a^2-a\rho\cos\phi}{R^2}\left[\frac{z+L}{\sqrt{(z+L)^2+R^2}} - \frac{z-L}{\sqrt{(z-L)^2+R^2}}\right]d\phi \tag{6}$$

Equation (6) is the expression for the axial component B_z of the magnetic induction strength of a single solenoid at any point in space. Due to the elliptic integral in the above equation, it is impossible to directly solve the expression of the axial component of the magnetic induction strength expressed as a finite primitive function. In order to reduce the number of calculations of the product function and to ensure sufficient accuracy. In this paper, a high-precision Gauss' quadrature formula is used to solve the above equation in order to obtain the magnetic flux density distribution of a single solenoid at any point in space. In this paper, the 4-node Gaussian product formula is chosen, and in order to increase the calculation accuracy, the integration interval is divided into 15 small intervals for calculation [29], and (6) can be written as follows

$$\begin{aligned}\int_a^b f(x)dx &= \sum_{k=0}^{14}\sum_{i=1}^{4}\frac{b_k-a_k}{2}\lambda_i f(x_i)\\ x_i &= \left((b_k+a_k)/2+(b_k-a_k)/2\right)t_i, \quad i=1,2,..,4\\ b_k &= (k+1)\,\pi/15\\ a_k &= k\pi/15\\ k &= 0,1,2\ldots,14\end{aligned} \tag{7}$$

where $f(x) = B_{2z}$, x_i is the nodes, λ_i is the weights. Substituting (6) into (7), the expression for the axial component of the magnetic flux density of a single solenoid with its geometric center at the origin is given by

$$\begin{aligned}B_{2z} &= \int_0^{\pi}\frac{a^2-a\rho\cos\phi}{R^2}\left[\frac{z+L}{\sqrt{(z+L)^2+R^2}} - \frac{z-L}{\sqrt{(z-L)^2+R^2}}\right]d\phi\\ &= \frac{\mu_0 nI}{2\pi}\left\{\sum_{k=0}^{14}\frac{b_k-a_k}{2}\sum_{i=1}^{4}\lambda_i\left\{\frac{\frac{a^2-a\rho\cos\phi_i}{R_i^2}}{\left[\frac{z+L}{\sqrt{(z+L)^2+R_i^2}} - \frac{z-L}{\sqrt{(z-L)^2+R_i^2}}\right]}\right\}\right\}\\ \phi_i &= \left((b_k+a_k)/2+(b_k-a_k)/2\right)t_i\\ R_i &= a^2+\rho^2-2a\rho\cos\phi_i\end{aligned} \tag{8}$$

The Gauss' quadrature formula has high algebraic accuracy and stable numerical results. The greater the number of nodes and intervals in the Gauss' quadrature formula, the more computationally intensive it is. 4-node 15 intervals can satisfy the computational requirements, as demonstrated below. To ensure the validity of (8), its computational accuracy can be calibrated by comparing the results obtained from different numbers of integration intervals. Using a single solenoid with a radius and axial length of 1 m as an example, the coefficient $\mu_0 nI$ in (8) is set to 1. This paper focuses on studying the magnetic field in the far-axis region of the column magnetron sputtering device, and therefore the coefficient is set to $\rho = 0.8$ m. Table 1 presents the results of the calculation for (8) using 15, 16, and 50 integral intervals.

Table 1 shows that increasing the number of integration intervals to 50 still results in 6 effective digits for the calculation results at 15 intervals. This indicates that the data from 15 intervals meets the required level of accuracy for subsequent calculations.

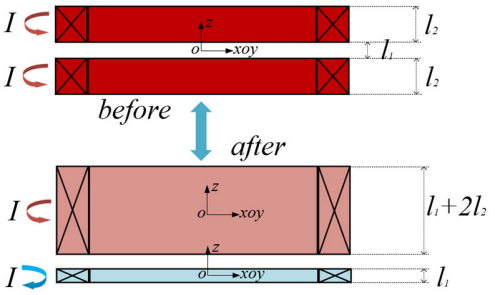

FIGURE 7. Schematic diagram of the equivalent method.

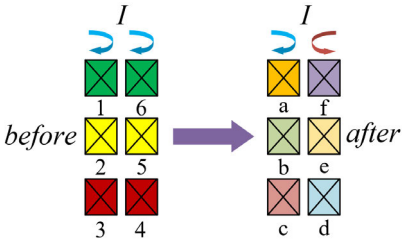

FIGURE 8. Schematic diagram of the equivalent method for six sets of solenoids.

C. ANALYTICAL MODEL OF THE MAGNETIC FIELD DISTRIBUTION IN AN AXISYMMETRIC SOLENOIDAL SYSTEM

Groups 1 and 6, Groups 2 and 5, and Groups 3 and 4 of the six sets of solenoids are symmetrical about the xoy plane. Two solenoids with plane symmetry consist of two identical solenoids placed symmetrically about the same axis. The two solenoids, shown in red at the top of Fig.7, are identical and symmetric about the xoy plane. The geometric centers of the two solenoids are not at the origin of the coordinate system; the axial spacing is l_1, and the axial length of each solenoid is l_2. From the perspective of generating a magnetic field, it can be analyzed as equivalent to the two solenoid structures at the bottom of Fig.7. Equivalent principle shown in Fig.7, from Fig.7 below the axial length of l_1+2l_2 solenoids to remove the axial length of l_1 solenoids after the remaining structure is Fig.7 above the solenoid structure. The four solenoids have the same number of turns per unit length of n, and the direction of the current is shown in Fig.7. The two structures produce the same magnetic field. This equivalent treatment can be the original geometric center that is not in the same point of the six groups of solenoid structure, equivalent to the geometric center being at the origin of the six groups of solenoid structure. The expression for the axial component of the magnetic flux density of the excitation structure of the axisymmetric solenoid system can be calculated directly by (8) and the principle of magnetic field superposition. And since the geometric centers are all at the origin, there is no need to introduce more unknown solenoid axial lengths for the calculation, which brings convenience to the calculation.

According to this equivalence method, the six sets of solenoids of the new excitation structure can be equated. The schematic diagram of the equivalence is shown in Fig.8, where on the left side are the six sets of solenoids before equivalence, whose numbers and colors are defined in Fig.2. On the right side, there are six groups of solenoids *a, b, c, d, e, f* after equivalence, and the geometric centers of the six groups of solenoids are at the origin. *a, b, c* have the same current direction as that of the axisymmetric solenoid system; and the current direction of *d, e, f* is opposite to that of the axisymmetric solenoid system. The number of turns n per unit length of the four groups of solenoids in each row in Fig.8 is the same as shown in (11), as shown at the bottom of the next page. Fig.8 is only a schematic diagram and does not reflect the actual size of the solenoids.

$$\begin{cases} \dfrac{N_1}{L_1} = \dfrac{N_6}{L_6} = \dfrac{N'_a}{L'_a} = \dfrac{N'_f}{L'_f} = n_1 \\ \dfrac{N_2}{L_2} = \dfrac{N_5}{L_5} = \dfrac{N'_b}{L'_b} = \dfrac{N'_e}{L'_e} = n_2 \\ \dfrac{N_3}{L_3} = \dfrac{N_4}{L_4} = \dfrac{N'_c}{L'_c} = \dfrac{N'_d}{L'_d} = n_3 \end{cases} \tag{9}$$

where N_1, $N_2 \ldots N_6$ and L_1, $L_2 \ldots L_6$ for the axisymmetric solenoid system six sets of solenoid turns, N'_1, $N'_2 \ldots N'_6$ and $L'_1, L'_2 \ldots L'_6$ are the number of turns and axial length of the six groups of equivalence solenoids, n_1, n_2, n_3 are the number of turns per unit length of the axisymmetric solenoid system, which are also equal to the number of turns per unit length of the six groups of equivalence solenoids, respectively.

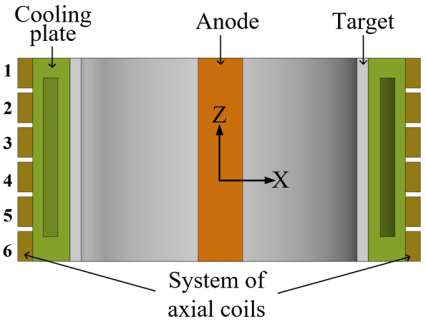

FIGURE 9. Schematic diagram of cylindrical magnetron sputtering equipment.

TABLE 2. Structural parameters for each component of magnetron sputtering equipment.

Component	Internal diameter(mm)	Outside diameter(mm)	Height(mm)
Target	105	115	136
Cooling plate	115	130	136

As a result, the axial component of the magnetic flux density generated in space by the excitation structure of the proposed axisymmetric solenoid system can be equated to the superposition of the axial components of the magnetic flux density generated in space by each of the six solenoids *a, b, c, d, e, f,* namely

$$B_z = B_{z1} + B_{z2} + B_{z3} + B_{z4} + B_{z5} + B_{z6} \tag{10}$$

where B_z is the axial component of the magnetic flux density generated by the excitation structure of the axisymmetric solenoid system at any point in space; B_{zk} is the axial component of the magnetic flux density jointly generated by the k-th equivalent post-solenoid at any point in space, and $k = 1, 2, 3, 4, 5, 6$. Substituting (8) into (10) gives the expression for the axial component of the magnetic flux density of the axisymmetric solenoid system at any point in space as where j denotes the number of solenoid groups.

IV. UNIFORM MAGNETIC FIELD DESIGN OF EXCITATION STRUCTURES FOR AXISYMMETRIC SOLENOIDAL SYSTEMS

In this section, firstly, the proposed excitation structure with analytical model is applied to the structure dimensions i13n [13], and a uniform magnetic field design is carried out on it, and a set of parameter combinations with high uniformity of axial magnetic field components are obtained as a result. The magnetic field generated by this excitation structure is then verified by simulation and compared and analyzed with that of several similar excitation structures, thus demonstrating the necessity and effectiveness of this

TABLE 3. Calculation results for parameters of an axisymmetric solenoid system.

Coil number	N	L (mm)
1	185.2985	19.96
2	94.7730	22.03
3	92.7210	21.01
4	92.7210	21.01
5	94.7730	22.03
6	185.2985	19.96

structure. Finally, the excitation structure of this size is actually fabricated, and the feasibility of this structure is proved by experimentally verifying that the structure can realize high uniformity of magnetic field distribution.

A. STRUCTURAL DIMENSIONS OF CYLINDRICAL MAGNETRON SPUTTERING EQUIPMENT

The magnetron sputtering system was designed with reference to the structural parameters in [13], and the structural schematic is shown in Fig.9, which shows the substrate, target, cooling pipe, and axisymmetric solenoid system in order from inside to outside. The structural parameters are listed in Table.2.

B. DESIGN OF UNIFORM MAGNETIC FIELDS

In this section, the proposed excitation structure with a uniform magnetic field is designed using the analytical model in the previous section. In magnetron sputtering, the plasma density can be controlled by the strength and distribution of the magnetic field. If the individual parameters of the excitation structure can be varied, a set of parameters can be used to achieve a uniform plasma density and thus a uniform coating.

The axial magnetic flux density distribution at 3 mm above the target material, the same as that in [13], is selected for the uniform magnetic field design. Since the product of the current and the number of turns together constitutes the electric component of the excitation structure, after fixing one of the current values and the number of turns, the other may still reflect the changing relationship of the electric component. Therefore, before calculating, the six sets of solenoid current value is fixed at 1 A, with the number of turns as an adjustable variable reflecting the change of the electrical component. The structural parameters of the magnetron sputtering equipment in the previous section are substituted into (11), i.e., ρ =102 mm; the radius of the six solenoids is unified as a = 130 mm; to fix the axial length of the axisymmetric solenoid structure, the maximum axial length of the six solenoids is taken as L = 68 mm, and the expression for the distribution of the magnetic field of the axisymmetric solenoid system in the cylindrical cross-section whose inner radial coordinate is obtained.

Since the magnetic field generated by the solenoid is axisymmetric, it is only necessary to analyze the uniformity of the magnetic field distribution on the line of intersection

TABLE 4. Rounded axisymmetric solenoid system parameters.

Coil number	N
1	185
2	95
3	93
4	93
5	95
6	185

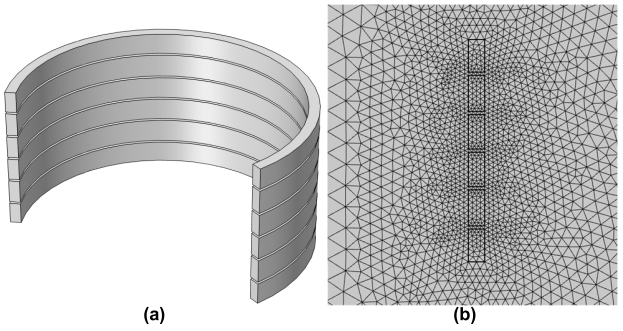

FIGURE 10. (a) Finite element simulation model of an axisymmetric solenoid system and (b) Mesh sectional diagram.

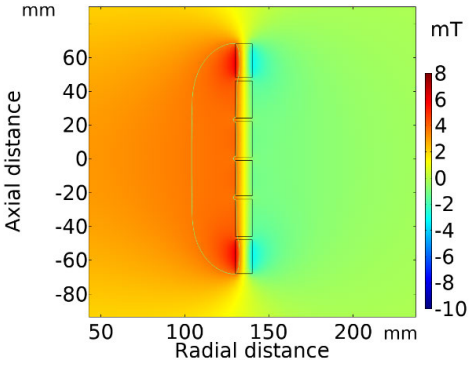

FIGURE 11. Magnetic flux density distribution map with contours for B_z = 3.36 mT.

$$B_z = \sum_{j=1}^{3}(-1)\frac{\mu_0 n_j I_j}{2\pi}\cdot\left\{\sum_{k=0}^{14}\frac{b_k-a_k}{2}\sum_{i=1}^{4}\lambda_i\left\{\frac{a^2-a\rho\cos\phi_i}{R_i^2}\left[\frac{z+L_j}{\sqrt{(z+L_j)^2+R_i^2}}-\frac{z-L_j}{\sqrt{(z-L_j)^2+R_i^2}}\right]\right\}\right\}$$
$$+\sum_{j=4}^{6}\frac{\mu_0 n_j I_j}{2\pi}\cdot\left\{\sum_{k=0}^{14}\frac{b_k-a_k}{2}\sum_{i=1}^{4}\lambda_i\left\{\frac{a^2-a\rho\cos\phi_i}{R_i^2}\left[\frac{z+L_j}{\sqrt{(z+L_j)^2+R_i^2}}-\frac{z-L_j}{\sqrt{(z-L_j)^2+R_i^2}}\right]\right\}\right\} \quad (11)$$

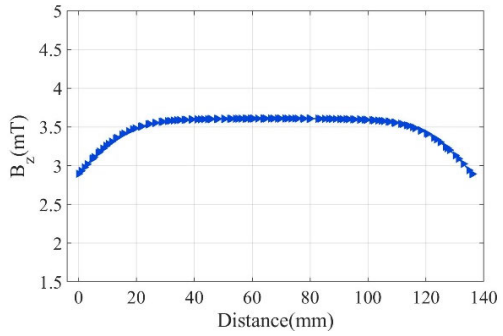

FIGURE 12. B_z distribution curve above the target.

TABLE 5. Parameters of the axisymmetric solenoid system with B_z = 30 mT.

Coil number	N	I (A)
1	172	9
2	88	9
3	86	99
4	86	9
5	88	9
6	172	9

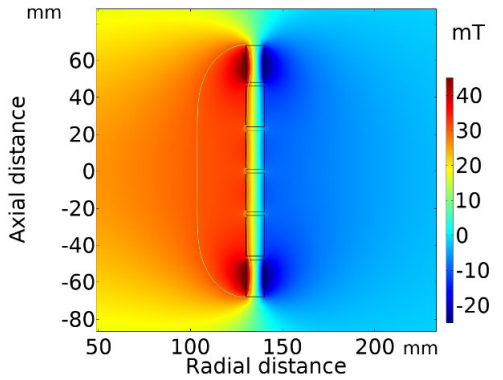

FIGURE 13. Magnetic flux density distribution map with contours for B_z = 30 mT.

between the xoz plane and the 102 mm cylindrical section. The magnetic field distribution on the intersection line of the cross section is rotated around the axis for one week to obtain the magnetic field distribution on the entire circumference in the same radial coordinates. (11) is an even function on the variable z. In order to make the B_z distribution at 3 mm above the target change minimally along the center position outward to obtain the parameter combination corresponding to the uniform magnetic field and realize the uniform magnetic field design, it is necessary to ensure that more even derivatives of (11) are equal to zero. A system of nonlinear differential equations is established to solve (12), i.e., a system of equations in which the derivatives of each order are zero.

$$\begin{cases} B_z^{(2)} = 0\Big|_{z=0} \\ B_z^{(4)} = 0\Big|_{z=0} \\ \cdots \\ B_z^{(2(n-1))} = 0\Big|_{z=0} \end{cases} \tag{12}$$

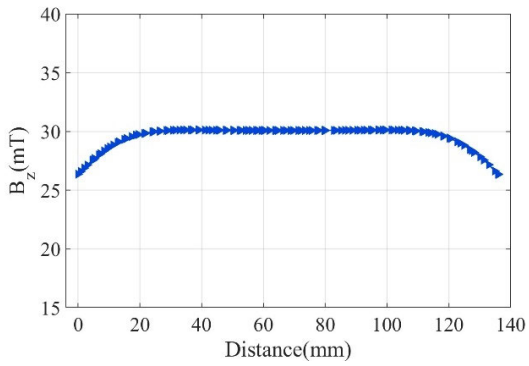

FIGURE 14. B_z distribution curve above the target.

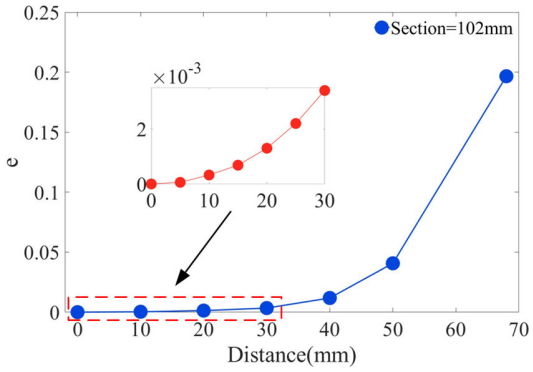

FIGURE 15. Comparison of deviation in magnetic field uniformity above the target.

The system of Eq. (12) is solved by the numerical method of [30]. The number of turns N and the axial length L of the axisymmetric solenoid system can be obtained from the equivalence relations described in Section III, and the results are shown in Table 3.

V. PERFORMANCE ANALYSIS AND EVALUATION OF EXCITATION STRUCTURES FOR AXISYMMETRIC SOLENOID SYSTEMS

A. AXIAL MAGNETIC FIELD DISTRIBUTION IN AXISYMMETRIC SOLENOID SYSTEMS

In this section, the parameter combinations obtained from the uniform magnetic field design in the previous section are verified by finite element simulation. The turns results obtained from the solution in the previous section contain decimals, which are rounded to the nearest whole number before substituting them into the finite element simulation, and the collated parameter values are shown in Table 4.

This finite element can simulate the 3D axisymmetric structure in 2D axisymmetric finite element, so this paper adopts its 2D axisymmetric finite element for the simulation and calculation work. Fig.10 (a) shows the finite element simulation model of the axisymmetric solenoid system, and Fig.10 (b) shows the mesh section.

The structure of the magnetron sputtering device was simulated by inputting the parameters of the axisymmetric

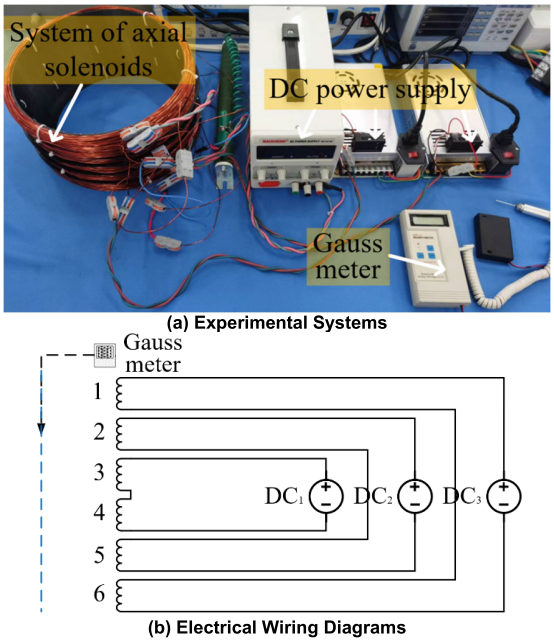

FIGURE 16. Experimental setup for axisymmetric solenoid excitation structure.

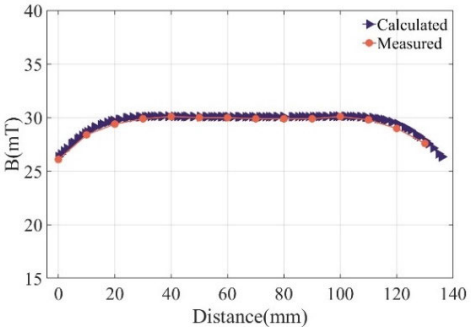

FIGURE 17. *B* distribution curve above the target.

TABLE 6. Structural parameters of the four excitation structures.

Component	Radius(mm)	Axial length(mm)
A ring-shaped permanent magnet	130	136
Three ring-shaped permanent magnets	130	136
Helmholtz coil	136	136
The long straight solenoid	130	136

solenoid system (number of turns and axial length) calculated in the previous section into the finite element software. The maximum value of the axial component of the flux density generated at the radial coordinates of the cylindrical cross-section (102 mm) is 3.63 mT. Fig.11 illustrates the flux density distribution of the excitation structure, featuring contours of the axial component with a density of 3.63 mT, along with the curve depicting the distribution of the axial component in the radial coordinates of the cylindrical cross-section (102 mm).

From Fig.11, it can be seen that on the contour line of $B_z =$ 3.36 mT, the axial middle region has very little variation and high uniformity, which can realize the magnetic field uniformity over a large range of the target surface. And in Fig.12, it can be observed that the axial component distribution curve of the magnetic flux density generated on a cylindrical cross section with radial coordinates of 102 mm is uniform over a large range, providing a more idealized axial magnetic flux density distribution for magnetron sputtering equipment.

Referring to the analysis of the magnitude of magnetic field required for magnetron sputtering in [13], the axial magnetic field component distribution at $B_z = 30$ mT will be used as the evaluation criterion for magnetic field uniformity in the subsequent paper. Since the magnetic field is proportional to the number of ampere-turns, the number of ampere-turns is adjusted. The adjusted data are those shown in Table 5.

Calculate the above data in the finite element software to obtain the magnetic flux density distribution map of the excitation structure at this time and the contour line of the magnetic flux density axial component of 30mT, as well as to obtain the distribution curve of the axial component of the magnetic flux density generated by its radial coordinate of 102mm cylindrical cross-section. Fig.13 and Fig.14 similarly show the high uniformity of the magnetic field generated by the excitation structure proposed in this paper, with the B_z distribution on the 102mm cross section varying very little in the range of 20 mm-110 mm, and the magnetic field being almost tilt-free with a high rate of curve flattening.

B. COMPARISON OF MAGNETIC FIELD UNIFORMITY DEVIATION

Fig.14 cannot quantitatively reflect the size degree of curve uniformity deviation, so the concept of magnetic field distribution uniformity deviation is introduced:

$$e = \frac{B_z(z) - B_z(0)}{B_z(0)} \tag{13}$$

where e is the uniformity deviation, which is used to quantitatively analyze the degree of deviation of the axial magnetic field from the magnetic field at the center of the axis after the radial coordinates are fixed; $B_z(z)$ is the axial component of the magnetic flux density at any point in the axial direction; and $B_z(0)$ is the axial component of the magnetic flux density at the center position.

Since the excitation structure is symmetrical along the xoy plane, calculating the uniformity deviation on one side reflects the results on both sides. The magnitude of the uniformity deviation for the B_z distribution of the cross section at 3 mm from the target surface is shown in Fig.15.

From Fig.15, it can be seen that the magnetic field uniformity deviation of the axisymmetric solenoid system is very small and uniform. The magnetic field uniformity deviation is 0.032% in the range of ±10 mm, 0.13% in the range of ±20 mm, 0.34% in the range of ±30 mm, 1.18% in the range of ±40 mm, 4.17% in the range of ±50 mm, and 19.66% in

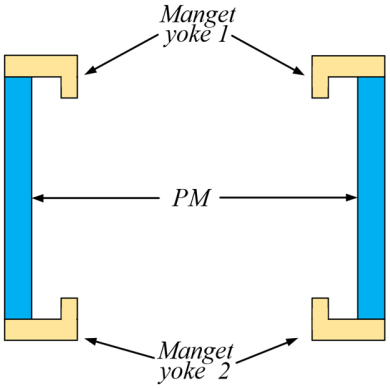

FIGURE 18. Schematic diagram of the excitation structure of a ring-shaped permanent magnet.

TABLE 7. Material parameters of a ring-shaped permanent magnet excitation structure.

Materials	Remanence flux density (T)	Relative permeability
Pm	1.11	1.05
Manget yoke	/	4000

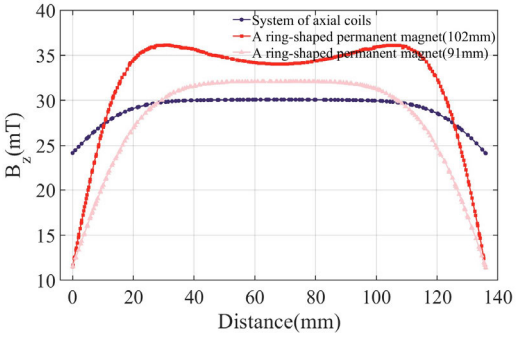

FIGURE 19. B_z distribution curve above the target.

the range of ±68 mm. The analysis of the uniform deviation of the magnetic field distribution shows that the excitation structure and analytical model proposed in this paper can achieve high uniformity of the magnetic field distribution on the target surface, proving the feasibility of this structure and method.

C. EXPERIMENTAL VERIFICATION OF MAGNETIC FIELD DISTRIBUTION

To demonstrate the method's feasibility and enable precise data measurement, this paper includes a related experiment. Fig.16 displays the experimental equipment. The experimental equipment comprises three sets of DC power supplies, six sets of solenoids, and a Gaussmeter for measurement. Additionally, an ABS plastic cylindrical support column is used, with each set of DC power supplies being connected to a different power supply model: the S-360-12, S-480-24, and MS-3010D. The Gaussmeter used for measurement is the SHT-V model, which has an accuracy of 0.1 mT. The support

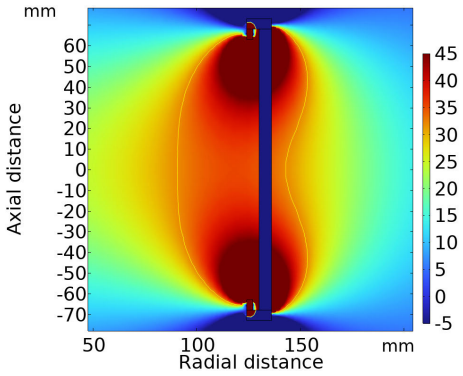

FIGURE 20. Magnetic flux density distribution map with contours for $B_z = 32$ mT.

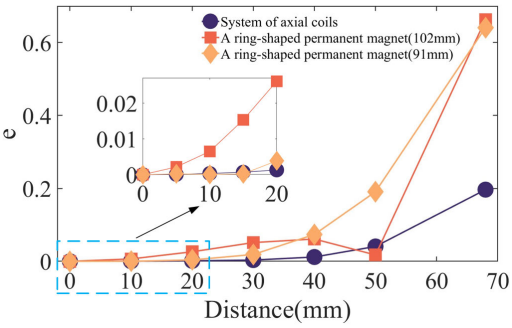

FIGURE 21. Comparison of deviation in magnetic field uniformity above the target.

column is cylindrical and measures 136 mm in height, with an inner diameter of 128 mm and an outer diameter of 130 mm.

The cylindrical support column was wound with enameled copper wires, and spacers were inserted to adjust the spacing of the solenoid groups. Six sets of solenoids were divided into three circuits and fed by three DC supplies, each with a branch current of 9 A. A Gaussmeter was used to measure the constant magnetic field. The magnetic field was measured using a Gaussmeter as a measuring instrument for the constant magnetic field. Measurements were taken at 1 cm intervals on the axis, 28 mm from the inner surface of the cylindrical support. This corresponds to the position 3 mm above the target surface in the magnetron sputtering equipment. A total of 14 points were measured.

The comparison curves in Fig.17 depict the magnetic flux density vector values since the Gaussmeter provides measurements as magnetic flux density vector values at discrete points along the axial direction, rather than specifically the axial component of the magnetic flux density vector values. As shown in Figure 17, the data are consistent, demonstrating the feasibility and correctness of the method presented in this paper.

VI. COMPARISON AND ANALYSIS OF SIMILAR EXCITATION STRUCTURES

This section compares four excitation structures for cylindrical magnetron sputtering devices with the proposed excitation structure. The four excitation structures are a ring-shaped

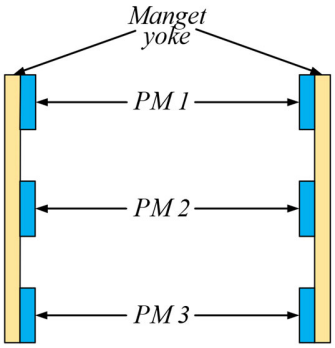

FIGURE 22. Schematic diagram of the excitation structure of three ring-shaped permanent magnets.

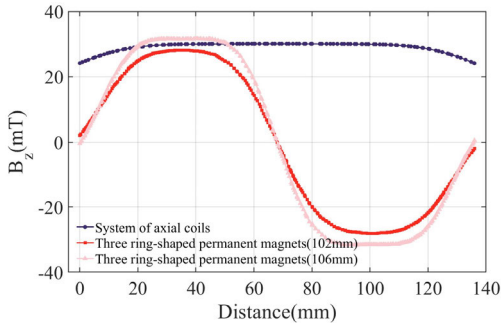

FIGURE 23. B_z distribution curve above the target.

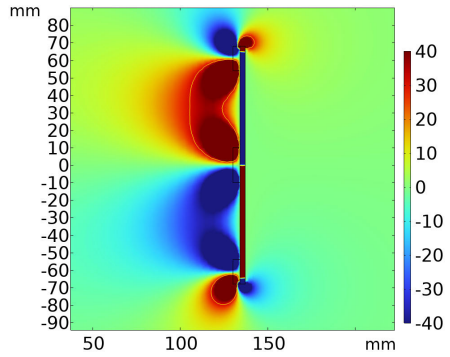

FIGURE 24. Magnetic flux density distribution map with contours for $B_z = 31$ mT.

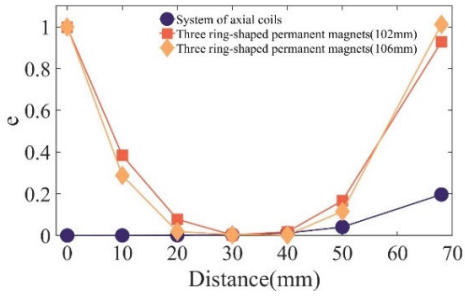

FIGURE 25. Comparison of deviation in magnetic field uniformity above the target.

permanent magnet, the three ring-shaped permanent magnets, the Helmholtz coil and the long straight solenoid. a ring-shaped permanent magnet, the three ring-shaped permanent magnets and the long straight solenoid share the same radius and axial length as the axisymmetric solenoid system discussed in the previous section. The radius is 130 mm and the axial length is 136 mm. The Helmholtz coil has special design requirements, so its radius and axial length are taken to be 136 mm. The magnetic field of approximately 30 mT was produced by adjusting the three excitation structures. Table.6 displays the structural parameters of these structures.

A. COMPARISON OF AXIAL MAGNETIC FIELDS OF A RING-SHAPED PERMANENT MAGNET

Fig.18 presents a schematic diagram of the excitation structure of a ring-shaped permanent magnet with yokes positioned at the upper and lower ends of the magnet. Table.7 displays the material parameters of a ring-shaped permanent magnet excitation structure.

Fig.19 displays a comparison between the distribution curve of the axial magnetic field of the axisymmetric solenoid system and that of a ring-shaped permanent magnet. The figure displays two axial magnetic field distribution curves for a ring-shaped permanent magnet at cross-sections of 102 mm and 91 mm. The 102 mm cross-section is the target position discussed in this paper, while the 91 mm cross-section is where the excitation structure of a ring-shaped permanent magnet generates a highly homogeneous magnetic field. The axial magnetic field distribution in the 102 mm section is non-uniform, exhibiting a wavy shape between 20-120 mm and less horizontal area. Additionally, the magnitude of the magnetic field distribution decreases significantly on both sides. In contrast, the axial magnetic field distribution of the 91 mm section has high uniformity in the 40-100 mm interval, but the same rapid drop in amplitude occurs on both sides. The higher homogeneity and wide range of occupancy of a ring-shaped permanent magnet proves the feasibility of this structure, but the large volume of the ring makes it more difficult to transport and install, and more suitable for small magnetron sputtering equipment. Fig.20 shows the magnetic flux density distribution of a ring-shaped permanent magnet with the magnetic flux density contours for an axial component of 32 mT. It is evident that the magnetic field exhibits uniformity.

In order to quantitatively compare the magnetic field distribution uniformity of a ring-shaped permanent magnet excitation structure with that of the axisymmetric solenoid system excitation structure. The analysis in Fig.21 examines the deviation from uniformity in the distribution of the magnetic field for both.

Fig.21 shows a comparison of the deviation in axial magnetic field uniformity between the two excitation configurations. In the 91 mm cross-section, the uniformity of a ring-shaped permanent magnet is higher. The axial magnetic field has a uniform deviation rate of 0.006% within the range of ±10 mm. The deviation of magnetic field

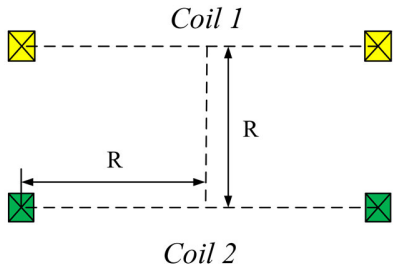

FIGURE 26. Schematic diagram of the excitation structure of the Helmholtz coil.

TABLE 8. Structure parameters of the Helmholtz coil excitation structure.

Component	Current (A)	Turns
Coil 1	9	450
Coil 2	9	450

uniformity is 0.38% within the range of ±20 mm. The deviation of magnetic field uniformity is 1.87% within the range of ±30 mm. The deviation of magnetic field uniformity is 7.36% within the range of ±40 mm. The deviation of magnetic field uniformity is 19.09% within the range of ± 50mm. The deviation of magnetic field uniformity is 64.13% within the range of ±68 mm. The uniformity of the excitation structure at 50 mm for a ring-shaped permanent magnet of 102 mm cross-section deviates by only 1.73%. This deviation is attributed to the magnet's wavy axial magnetic field distribution. Fig.21 shows that the axisymmetric solenoid system has a better uniformity of magnetic field distribution than a ring-shaped permanent magnet excitation structure. However, a ring-shaped permanent magnet can also achieve high uniformity of magnetic field distribution within ±30 mm.

B. COMPARISON OF AXIAL MAGNETIC FIELDS OF THREE RING-SHAPED PERMANENT MAGNETS

Fig.22 displays a permanent magnet excitation structure consisting of three ring-shaped permanent magnets distributed longitudinally, followed by a magnetic yoke to guide the magnetic field. The material parameters for this excitation structure are identical to those of a ring-shaped permanent magnet, as listed in Table 7.

Fig.23 shows the distribution curve of the axial magnetic field of the axisymmetric solenoid system compared to the axial magnetic field of three ring-shaped permanent magnets. The figure displays two three ring-shaped permanent magnets curves that represent the axial magnetic field distribution at cross sections 102 mm and 106mm. The 102 mm cross section is the target position discussed in this paper, while the 106mm cross section is where the excitation structure of three ring-shaped permanent magnets generates a highly uniform magnetic field. The axial magnetic field on the 106 mm cross section has high uniformity in the range of 20-50 mm and 90-110 mm, but the design of its multi-magnet ring structure

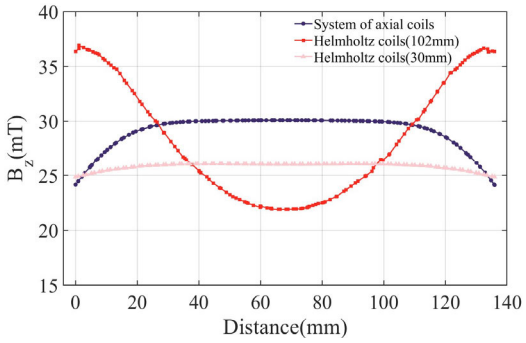

FIGURE 27. B_z distribution curve above the target.

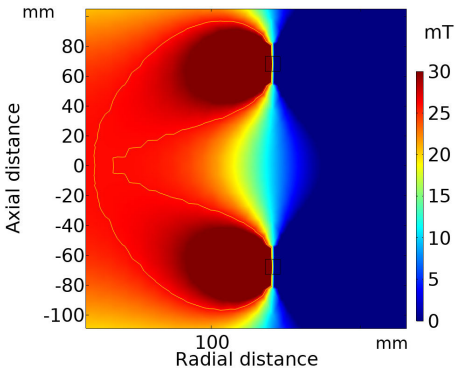

FIGURE 28. Magnetic flux density distribution map with contours for B_z = 26.02 mT.

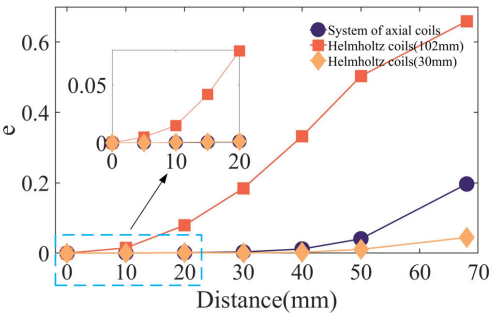

FIGURE 29. Comparison of deviation in magnetic field uniformity above the target.

leads to the inevitable occurrence of three inhomogeneous regions with rapidly decreasing magnetic field amplitude, and the sputtering effect occurring in these regions will be affected.

Fig.24 shows the magnetic flux density distribution of three ring-shaped permanent magnets with the magnetic flux density contours for an axial component of 31 mT. It can be seen that the contours are distributed in an arc, with high uniformity in the central region of the arc, but poor uniformity of the magnetic field in the centre of the device.

In order to quantitatively compare the magnetic field uniformity of the two excitation structures, the deviation from

TABLE 9. Long straight solenoid structural parameters.

Component	Current(A)	Turns
Long straight solenoid	9	680

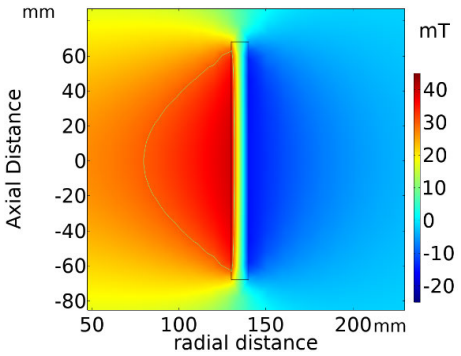

FIGURE 30. Magnetic flux density distribution map with contours for $B_z = 30$ mT.

the uniformity of the magnetic field distribution was compared. However, due to the peculiarity of the magnetic field distribution curve of three ring-shaped permanent magnets excitation structure, taking the origin as the reference point according to equation (13) cannot reflect the uniformity change. Therefore, three ring-shaped permanent magnets excitation structure uniformity deviation formula is adjusted, the adjusted formula is

$$e = \frac{B_z(z) - B_z(35)}{B_z(35)} \tag{14}$$

where is the value of the axial flux density at 35 mm from the origin in the axial direction in Fig.23, and the deviation of the uniformity of the magnetic field distribution of the two excitation structures was analyzed, and the results are shown in Fig.25.

Fig.25 shows a comparison of the axial magnetic field uniformity deviation of the two excitation structures. It is evident that the uniformity deviation value of three ring-shaped permanent magnets excitation structure increases significantly in the range of 0-20 mm and 50-70 mm, resulting in poor uniformity. The axial magnetic field of three ring-shaped permanent magnets deviates uniformly within ±10 mm of the 106 mm cross-section with a 99.92% accuracy. The deviation of magnetic field uniformity is 28.78% within the range of ±20 mm. The deviation of magnetic field uniformity is 0.39% within the range of ±30 mm. The deviation of magnetic field uniformity is 0.24% within the range of ±40 mm. The deviation of magnetic field uniformity is 11.57% within the range of ±50 mm. The deviation of magnetic field uniformity is 101.17% within the range of ±68 mm. The data presented above indicate that the excitation structure of three ring-shaped permanent magnets has a less effective uniform magnetic field and fewer uniform regions compared to the axisymmetric solenoid system excitation structure.

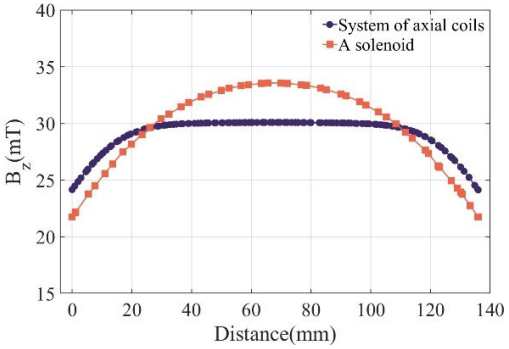

FIGURE 31. B_z distribution curve above the target.

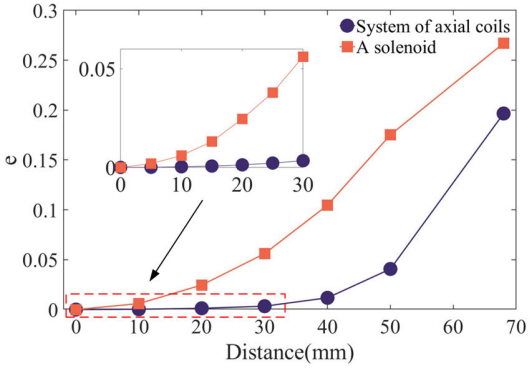

FIGURE 32. Comparison of deviation in magnetic field uniformity above the target.

C. COMPARISON OF AXIAL MAGNETIC FIELDS OF HELMHOLTZ COILS

Fig.26 presents a schematic diagram of the Helmholtz coil excitation structure. This structure consists of two axisymmetric solenoids that are longitudinally distributed. Both coils have the same current magnitude and direction, and the coil radius is equal to the axial length, meeting the design requirements. Table 8 displays the parameters of the excitation structure.

Fig.27 displays a comparison between the distribution curve of the axisymmetric solenoid system and the axial magnetic field distribution curve of the Helmholtz coil. The figure displays two Helmholtz coil curves depicting the axial magnetic field distribution at cross sections 102 mm and 30 mm. The 102 mm cross section is the target location discussed in this paper, while the 30 mm cross section is where the Helmholtz coil excitation structure generates a highly uniform magnetic field. The magnetic field at the 102 mm cross section exhibits poor uniformity with almost no uniform region. In contrast, the 30 mm cross-section exhibits an axial magnetic field distribution with a high degree of homogeneity. The magnetic field does not decrease significantly on either side of this section. However, it is important to note that the excitation structure has a radius of 136 mm and an axial length at this point. Additionally, a highly uniform magnetic field distribution cross-section appears near 30 mm.

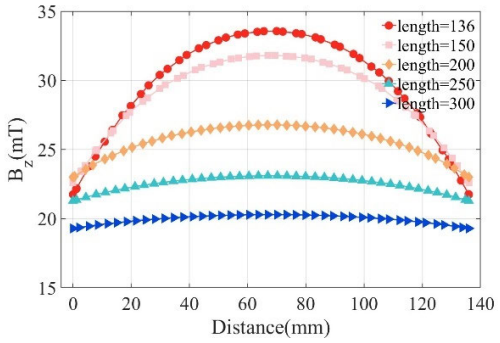

FIGURE 33. B_Z distribution curve above the target.

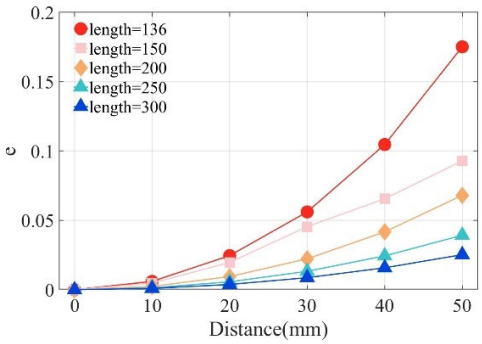

FIGURE 34. Comparison of deviation in magnetic field uniformity above the target.

This suggests that when a Helmholtz coil excitation structure is used in a magnetron sputtering device, the target-base spacing inside it is substantially compressed and more space is required for the mounting of the excitation structure.

Fig.28 shows the magnetic flux density distribution of the Helmholtz coil with the magnetic flux density contours for an axial component of 26.02 mT. It can be observed that the region of uniform contour is in close proximity to the central axis. This observation suggests that the uniform magnetic field generated by the Helmholtz coil is primarily distributed in the near-axis region, while the far-axis region exhibits poor uniformity in axial magnetic field distribution.

In order to quantitatively compare the magnetic field uniformity of the two excitation structures, the deviation from the uniformity of the magnetic field distribution was compared. Fig.29 displays the results.

Fig.29 shows that the Helmholtz coil magnetic field uniformity deviation is at its worst at the 102 mm cross-section. Additionally, the uniformity of the Helmholtz coil magnetic field distribution is higher at the 30 mm cross-section compared to that of the axisymmetric solenoid system. The axial magnetic field of the Helmholtz coil deviates uniformly within ±10 mm of the 30 mm cross-section with a 0.0099% accuracy. The deviation of magnetic field uniformity is 0.12% within the range of ±20 mm. The deviation of magnetic field uniformity is 0.092% within the range of ±30 mm. The deviation of magnetic field uniformity is 0.23% within the range of ±40 mm. The deviation of magnetic field uniformity is 1.06% within the range of ±50 mm. The deviation of magnetic field uniformity is 4.45% within the range of ±68 mm. The effectiveness of Helmholtz coils in achieving a highly uniform magnetic field distribution in the near-axis region is once again demonstrated. However, the axial magnetic field distribution in the far-axis region is poor.

D. COMPARISON OF AXIAL MAGNETIC FIELDS OF THE LONG STRAIGHT SOLENOID

In this subsection, a long straight solenoid is analyzed in comparison to the magnetic field distribution generated by an axisymmetric solenoid system. This long straight solenoid has the same radius and axial length as the axisymmetric solenoid system in the previous section, and the number of ampere-turns is set so that it can generate a magnetic field of approximately 30 mT. The design parameters of the long straight solenoid are shown in Table 9.

TABLE 10. Data sheet for deviation from magnetic field uniformity for long straight solenoids.

Axial length	Axial distance				
	10 mm	20 mm	30 mm	40 mm	50 mm
136 mm	0.6%	2.46	5.61%	10.47%	17.52%
150 mm	0.48%	1.97%	4.55%	6.56%	9.29%
200 mm	0.24	0.95%	2.23%	4.17%	6.81%
250 mm	0.14%	0.57%	1.33%	2.44%	3.93%
300 mm	0.094%	0.38%	0.87%	1.58%	2.53%

Fig.30 shows the magnetic flux density distribution of the long straight solenoid with the magnetic flux density contours for an axial component of 30 mT. Comparison with the axial magnetic field contours of the axisymmetric solenoid system in the previous section clearly shows that the long straight solenoid produces a less uniform magnetic field and requires more ampere-turns to achieve the specified field size. Fig 31 shows the plot of the B_z distribution of the axisymmetric solenoid system at 3 mm above the target compared to the long straight solenoid structure.

From Fig.31, it can be seen that the axial magnetic field of the long straight solenoid has an arcuate distribution with poor uniformity and less horizontal region. Compared with the long straight solenoid, the axisymmetric solenoid system produces a higher uniformity of the axial magnetic field. In magnetron sputtering, the increased uniformity of the magnetic field on the target surface will increase the utilization of the target material and reduce the downtime for target replacement.

For a more quantitative comparison of the uniformity of the magnetic field distribution on the target surface of the two, the deviation of the uniformity of the magnetic field distribution of the two was calculated, as shown in Fig.32.

The uniform deviation rate of the axial magnetic field of the long straight solenoid in Fig.32 is significantly larger than that of the axisymmetric solenoid system. The axial magnetic field of the long straight solenoid deviates uniformly within

±10 mm of the 30 mm cross-section with a 0.6% accuracy. The deviation of magnetic field uniformity is 2.46% within the range of ±20 mm. The deviation of magnetic field uniformity is 5.61% within the range of ±30 mm. The deviation of magnetic field uniformity is 10.47% within the range of ±40 mm. The deviation of magnetic field uniformity is 17.52% within the range of ±50 mm. The deviation of magnetic field uniformity is 26.7% within the range of ±68 mm. In the range of 18mm-118mm, the magnetic field uniformity deviation rate of the axisymmetric solenoid system is one order of magnitude smaller than that of the long straight solenoid. This demonstrates that the axisymmetric solenoid system produces a higher uniformity of axial magnetic field compared to the long straight solenoid excitation. The paper demonstrates that the proposed excitation structure and analytical model can achieve a high level of uniformity in the magnetic field distribution on the target surface, resulting in increased target utilization.

E. LONG STRAIGHT SOLENOID UNIFORMITY ANALYSIS

Long straight solenoids are known to produce a uniform B_z distribution in the internal axial direction. Therefore, in this subsection, the axial length L of the long straight solenoid in the previous section is extended to achieve a higher uniformity of B_z distribution. And this is studied and analyzed.

The axial lengths of the long straight solenoid excitation structures were set at 136 mm, 150 mm, 200 mm, 250 mm, and 300 mm. The length of 136 mm corresponds to the axial length of the magnetron sputtering equipment in this paper, while the other parameters remained constant. Magnetic field simulations were conducted for each of the five sets of structures. Figure 33 illustrates a comparison of the B_z distribution curves at 3 mm above the target.

Figure.33 shows that increasing the axial length of the long straight solenoid results in a smoother and more uniform distribution of the axial magnetic field component B_z. This trend is also reflected in Fig.34, and Table.10 lists the magnetic field uniformity deviations of the five structures.

Table 10 shows that the long straight solenoid must have an axial length of 300 mm or more to approach the uniformity of the magnetic field distribution generated by the axisymmetric solenoid system proposed in this paper. However, increasing the axial length of the long straight solenoid reduces the size of the generated magnetic field, requiring the addition of more turns or currents to achieve the target magnetic field size. Fig.34 demonstrates the comparison of the deviation rate of B_z magnetic field uniformity at 3 mm above the target for five groups of structures.

This supports the claim that the excitation structure proposed in this paper is more suitable for generating a uniform B_z distribution for magnetron sputtering equipment compared to the long straight solenoid structure.

VII. CONCLUSION

This paper analyzes the desired magnetic field distribution characteristics of magnetron sputtering equipment, and accordingly proposes and calculates a uniform magnetic field excitation structure and an analytical model of the magnetic field applied to cylindrical magnetron sputtering. The proposed excitation structure's uniform magnetic field design was carried out using the analytical model. The uniform magnetic field results obtained were verified and analyzed using both simulation and experimental methods. The conclusions are as follows:

1. The study confirms that the newly proposed excitation structure achieves a high level of uniformity in the axial magnetic field distribution, with a deviation of less than 4.2% within the range of ±50mm. The proximity of the magnetic field's axial component to the midpoint of the axis directly correlates with its uniformity. Within a range of ±10mm, the deviation of the magnetic field's uniformity is only 0.032%. However, uniformity decreases at the axial ends. The highly uniform axial magnetic field distribution in the axisymmetric solenoid system results from the ability to adjust neighboring solenoids through the uniform magnetic field design, allowing for parameter adjustments and magnetic field interaction.

2. A ring-shaped permanent magnet can generate axial magnetic fields with high uniformity and a wide range of occupation ratios. There is a 7.36% maximum deviation in uniformity within ±40 mm. However, there is a rapid decrease in the magnetic field on both sides of the curve. This results in a deviation of magnetic field uniformity of 19.09% at ±50 mm, which can cause poor sputtering uniformity at both ends. The solenoid system with axisymmetric design, however, provides a more uniform distribution of magnetic field on both sides. This is due to the fact that its electrical load is small in the middle and large at both ends in the axial direction. Three ring-shaped permanent magnets can generate two curved magnetic fields in a cylindrical cross-section. However, the multiple magnetic ring structure design results in the inevitable occurrence of multiple segments with inhomogeneous regions, where the magnetic field amplitude decreases rapidly. Deviation values higher than 99% were observed at ±10 mm and ±68 mm, indicating a lack of uniformity. These areas will be affected by the sputtering effect. The axisymmetric solenoid system has a better overall magnetic field uniformity, with a deviation of less than 19.66% within the range of ±68 mm.

3. The Helmholtz coil excitation structure can generate a highly uniform magnetic field distribution in the near-axis region. The maximum deviation from uniformity over the entire axial length is less than 5%. However, currently, the excitation coil is mounted 136 mm away from the centre axis, and the magnetic field uniformity in the far axis region is very unsatisfactory. Comparison of the two excitation structures reveals that the axial magnetic field distribution of the long straight solenoid is curved and lacks uniformity. In contrast, the axisymmetric solenoid system, with fewer ampere-turns under the same axial length, achieves a higher level of uniformity in the axial magnetic field. Within the range of ±50 mm, the axial magnetic field deviation of the axisymmetric solenoid system is only 0.23 times that of the long

straight solenoid. This significant difference arises from the long straight solenoid's inability to regulate the magnetic field distribution across different regions, unlike the multi-group solenoid structure. A solenoid with an axial length of 300 mm produces a magnetic field uniformity similar to that of a 136 mm axisymmetric solenoid system. To achieve the same magnitude of B_z, an axisymmetric solenoid system requires fewer turns than a long straight solenoid.

REFERENCES

[1] S. Kim and N.-H. Kim, "Electronic structure and thermoelectric properties of Mg_2Sn films fabricated by using co-sputtering process with stoichiometric modification," *IEEE Access*, vol. 10, pp. 380–390, 2022.

[2] J.-C. Chou, P.-F. Chen, P.-H. Yang, C.-H. Lai, P.-Y. Kuo, Y.-H. Nien, S.-W. Zhuang, R.-H. Syu, and Y.-H. Huang, "Modification of dye-sensitized solar cells with sputter-deposited titanium dioxide blocking layer for enhanced photovoltaic performance under different illuminations," *IEEE Access*, vol. 11, pp. 98082–98092, 2023.

[3] Y. Lu, C. Yang, H. Wang, L. Ma, M. Xu, and L. Xi, "Structure, principle, and application of magnetic field-assisted pulsed laser deposition: An overview," *Vacuum*, vol. 211, May 2023, Art. no. 111912.

[4] D. Vavassori, F. Mirani, F. Gatti, D. Dellasega, and M. Passoni, "Role of magnetic field and bias configuration on HiPIMS deposition of w films," *Surf. Coatings Technol.*, vol. 458, Apr. 2023, Art. no. 129343.

[5] W. Yu, X. Wang, H. Lu, H. Liu, and C. Jin, "3D-printed all-metal terahertz multibeam lens antenna based on photonic crystal," *IEEE Access*, vol. 11, pp. 41609–41617, 2023.

[6] G. Kaune, D. Hagedorn, and F. Löffler, "Magnetron sputtering process for homogeneous internal coating of hollow cylinders," *Surf. Coatings Technol.*, vol. 308, pp. 57–61, Dec. 2016.

[7] C.-T. Liu, M.-C. Lai, C.-C. Hwang, C.-H. Tu, L.-Y. Liu, and Y.-W. Hsu, "Enhancements of substrate deposition rate and target erosion profile in a DC magnetron sputtering system," *IEEE Trans. Magn.*, vol. 45, no. 10, pp. 4391–4394, Oct. 2009.

[8] C.-T. Liu, M.-C. Lai, and C.-C. Hwang, "Design assessments of a refined DC magnetron sputter with multiple magnetron arrangements," *IEEE Trans. Magn.*, vol. 46, no. 6, pp. 1614–1617, Jun. 2010.

[9] C.-T. Liu, C.-W. Chang, and C.-C. Hwang, "Smoother substrate deposition designs and process emulations of DC magnetron sputters," *IEEE Trans. Magn.*, vol. 48, no. 11, pp. 4432–4435, Nov. 2012.

[10] C.-T. Liu, H.-C. Yeh, H.-Y. Chung, and C.-C. Hwang, "Design assessments of a rectangular DC magnetron sputter for extended target life and faster sputtering," *IEEE Trans. Magn.*, vol. 50, no. 1, Jan. 2014, Art. no. 4002204.

[11] C.-T. Liu, C.-C. Hwang, and C.-W. Chang, "Optimal magnetic field path designs for enhanced depositions of DC magnetron sputter," *IEEE Trans. Magn.*, vol. 50, no. 11, pp. 1–4, Nov. 2014.

[12] H. Kawasaki, H. Nishiguchi, T. Furutani, T. Ohshima, Y. Yagyu, T. Ihara, M. Shinohara, and Y. Suda, "Coating of inner surface of cylindrical pipe for hydrogen entry prevention using plasma process," *Jpn. J. Appl. Phys.*, vol. 57, no. 1S, Jan. 2018, Art. no. 01AB02.

[13] D. Wang, C.-L. Cai, Q. Mi, L.-B. Wang, H.-C. Liu, and J. Hou, "Magnetic field simulation and structure design of cylindrical magnetron sputtering target," *Surf. Technol.*, vol. 52, no. 8, pp. 371–379, 2023.

[14] M. Gasab, H. Sugawara, T. Sato, and H. Fujiyama, "Tube inner coating of non-conductive films by pulsed reactive coaxial magnetron plasma with outer anode," *Coatings*, vol. 8, no. 3, Mar. 2018, Art. no. 115.

[15] R. Rane, A. Joshi, S. Akkireddy, and S. Mukherjee, "Comparative study of discharge characteristics and associated film growth for post-cathode and inverted cylindrical magnetron sputtering," *Pramana*, vol. 92, no. 4, Apr. 2019, Art. no. 55.

[16] S. Kim and K. H. Kim, "Effect of magnetic field arrangement of facing targets sputtering (FTS) system on controlling plasma confinement," *Coatings*, vol. 10, no. 4, Mar. 2020, Art. no. 321.

[17] T. Weichsel, U. Hartung, T. Kopte, G. Zschornack, M. Kreller, and A. Silze, "An inverted cylindrical sputter magnetron as metal vapor supply for electron cyclotron resonance ion sources," *Rev. Sci. Instrum.*, vol. 85, no. 5, May 2014, Art. no. 053301.

[18] S. S. Parhizgar, "The effect of substrate position during cylindrical DC magnetron sputtering on physical properties of Fe_7Co_3 thin film," *Trans. Indian Inst. Met.*, vol. 66, no. 3, pp. 201–205, Jun. 2013.

[19] H. Kakati and S. M. Borah, "Study of hysteresis behavior in reactive sputtering of cylindrical magnetron plasma," *Chin. Phys. B*, vol. 24, no. 12, Dec. 2015, Art. no. 125201.

[20] E. Darabi, N. Moghaddasi, and M. R. Hantehzadeh, "Mechanical properties of Ta-Al-N thin films deposited by cylindrical DC magnetron sputtering: Influence of N2% in the gas mixture," *Eur. Phys. J. Plus*, vol. 131, no. 6, Jun. 2016, Art. no. 187.

[21] T. Kretková, J. Hanuš, O. Kylián, P. Solař, M. Dopita, M. Cieslar, I. Khalakhan, A. Choukourov, and H. Biederman, "In-flight modification of Ni nanoparticles by tubular magnetron sputtering," *J. Phys. D, Appl. Phys.*, vol. 52, no. 20, May 2019, Art. no. 205302.

[22] M. H. Faruk, M. Ferdows, and E. E. Tzirtzilakis, "Hyperthermia temperature reduction in biomagnetic flow: Thermal transfer in Fe_3O_4-blood particle suspension with uniform and non-uniform effects," *Phys. Fluids*, vol. 35, no. 1, Jan. 2023, Art. no. 011902.

[23] X. Zhu, C. Liu, H. Su, Y. Miao, and H. Cheng, "Design of improved four-coil structure with high uniformity and effective coverage rate," *Heliyon*, vol. 9, no. 4, Apr. 2023, Art. no. e15193.

[24] Y. Öztürk and B. Aktas, "Generation of uniform magnetic field using a spheroidal helical coil structure," in *Proc. 9th Int. Conf. Magn. Superconducting Mater. (MSM)*, vol. 667, Antalya, Turkey, 2016, p. 012009.

[25] A. A. Bayazitov, Y. V. Fattakhov, A. R. Fakhrutdinov, and V. A. Shagalov, "A receiving coil for a specialized compact magnetic resonance imaging system," *Instrum. Experim. Techn.*, vol. 63, no. 6, pp. 875–879, Dec. 2020.

[26] M. D. Bird, I. R. Dixon, and J. Toth, "Large, high-field magnet projects at the NHMFL," *IEEE Trans. Appl. Supercond.*, vol. 25, no. 3, pp. 1–6, Jun. 2015.

[27] J. Chen, Z. Wu, G. Bao, L. Q. Chen, and W. Zhang, "Design of coaxial coils using hybrid machine learning," *Rev. Scientific Instrum.*, vol. 92, no. 4, Apr. 2021, Art. no. 045103.

[28] J. T. Gudmundsson, "Physics and technology of magnetron sputtering discharges," *Plasma Sources Sci. Technol.*, vol. 29, no. 11, Nov. 2020, Art. no. 113001.

[29] B. Dang, L. Yang, C. Liu, Y. Zheng, H. Li, R. Dang, and B. Sun, "A uniform linear multi-coil array-based borehole transient electromagnetic system for non-destructive evaluations of downhole casings," *Sensors*, vol. 18, no. 8, Aug. 2018, Art. no. 2707.

[30] V. E. Baranova, P. F. Baranov, S. V. Muravyov, and S. V. Uchaikin, "The production of a uniform magnetic field using a system of axial coils for calibrating magnetometers," *Meas. Techn.*, vol. 58, no. 5, pp. 550–555, Aug. 2015.

ZE-DA SU was born in Shenyang, Liaoning, China, in 1993. He received the M.S. degree from the School of Electrical Engineering, Shenyang University of Technology, China, in 2021, where he is currently pursuing the Ph.D. degree. His research interests include electromagnetic designs, electromagnetic theory, and vacuum coating-related research.

YUE-JUN AN was born in Changchun, Jilin, China, in 1962. He received the Ph.D. degree in electrical machine and electrical apparatus from Shenyang University of Technology, in 2005. Since 2009, he has been a Professor with the College of Electrical Engineering, Shenyang University of Technology. His research interests include the design of special motors, the numerical calculation of integrated physical fields in motors, the cooling systems of electric motors, and thermal modeling.

HUI AN was born in Shenyang, Liaoning, China, in 1989. He received the B.S. degree from the College of Electrical Engineering, Shenyang University of Technology, Shenyang, in 2012, and the M.S. degree from the College of Information Science and Engineering, Shenyang University of Technology, in 2017. His research interests include motor designs and automation control.

YAN-JUN LU was born in Penglai, Shandong, China, in 1990. She received the B.S. and M.S. degrees from the College of Mechanical Engineering and Automation, Northeastern University, Shenyang, China, in 2013 and 2015, respectively. Her research interests include the design and analysis of electrical machines and industrial machinery.

WEN-YU DENG was born in Xingning, Guangdong, China, in 1982. He received the B.S. degree from the College of Life Sciences, Shaanxi Normal University, in 2004. He is currently working with Shenyang China North Vacuum Equipment Company Ltd. and is a member of the Vacuum Metallurgy Committee of the Chinese Vacuum Society. His research interests include vacuum technology and the preparation, property testing and application of metallic materials.

LI-JUN QI was born in Chifeng, Inner Mongolia Autonomous Region, China, in 1981. He received the B.S. and M.S. degrees from the College of Chemistry and Chemical Engineering, Liaoning Normal University. He is currently working with Shenyang China North Vacuum Equipment Company Ltd., and is the Deputy Secretary General of the Vacuum Metallurgy Committee of the China Vacuum Society. His research interests include metal materials, vacuum technology, and surface treatment technology.

MING LI was born in Jinzhou, Liaoning, China, in 1987. He received the M.S. degree in electrical machines and electrical apparatus and the Ph.D. degree in electrical engineering from Shenyang University of Technology, in 2023. His research interests include electromagnetic design, thermal designs, and energetic behaviors of electric machines.